



Study of structural and ferromagnetic resonance properties of spinel lithium ferrite (LiFe_5O_8) single crystals

Cite as: J. Appl. Phys. **117**, 233907 (2015); <https://doi.org/10.1063/1.4922778>

Submitted: 24 February 2015 . Accepted: 06 May 2015 . Published Online: 19 June 2015

Neha Pachauri, Behrouz Khodadadi, Matthias Althammer, Amit V. Singh , B. Loukya, Ranjan Datta, Milko Iliev, Leonard Bezmaternykh , Irina Gudim, Tim Mewes, and Arunava Gupta



View Online



Export Citation



CrossMark

ARTICLES YOU MAY BE INTERESTED IN

[Structural and magnetic properties of lithium ferrite \(\$\text{LiFe}_5\text{O}_8\$ \) thin films: Influence of substrate on the octahedral site order](#)

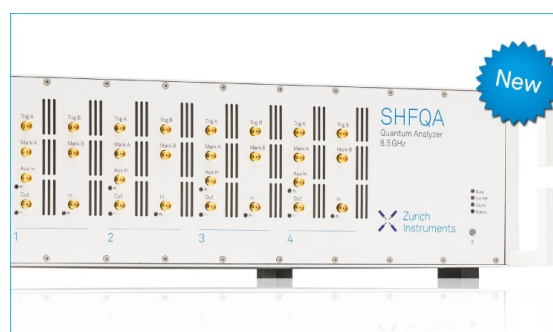
Applied Physics Letters **98**, 012507 (2011); <https://doi.org/10.1063/1.3533908>

[Magnetic properties of superparamagnetic lithium ferrite nanoparticles](#)

Journal of Applied Physics **98**, 124312 (2005); <https://doi.org/10.1063/1.2149493>

[Properties of Single-Crystal Lithium Ferrite Grown in the Ordered State](#)

Journal of Applied Physics **35**, 3320 (1964); <https://doi.org/10.1063/1.1713215>



Your Qubits. Measured.

Meet the next generation of quantum analyzers

- Readout for up to 64 qubits
- Operation at up to 8.5 GHz, mixer-calibration-free
- Signal optimization with minimal latency

Find out more



Study of structural and ferromagnetic resonance properties of spinel lithium ferrite (LiFe_5O_8) single crystals

Neha Pachauri,¹ Behrouz Khodadadi,¹ Matthias Althammer,² Amit V. Singh,² B. Loukya,³ Ranjan Datta,³ Milko Iliev,⁴ Leonard Bezmaternykh,⁵ Irina Gudim,⁵ Tim Mewes,¹ and Arunava Gupta^{2,a)}

¹*Department of Physics and Astronomy, MINT Center, University of Alabama, Tuscaloosa, Alabama 35487, USA*

²*Department of Chemistry, MINT Center, University of Alabama, Tuscaloosa, Alabama 35487, USA*

³*International Centre for Materials Science, Jawaharlal Nehru Centre for Advanced Scientific Research, Bangalore 560064, India*

⁴*Texas Center for Superconductivity and Department of Physics, University of Houston, Houston, Texas 77204, USA*

⁵*Kirensky Institute of Physics, SB RAS, Akademgorodok, Krasnoyarsk 660036, Russia*

(Received 24 February 2015; accepted 6 May 2015; published online 19 June 2015)

The effect of B-site cation ordering on the room temperature structural and ferromagnetic resonance (FMR) properties of single crystal spinel lithium ferrite (LiFe_5O_8 , LFO) have been investigated. A detailed microstructural analysis is done through X-ray diffraction, polarized Raman spectroscopy, and transmission electron microscopy (TEM) to examine the effect of post-annealing on the B-site cation ordering. The X-ray diffraction pattern of the as-grown crystal indicates a disordered state of the crystal. However, the annealed sample shows additional superlattice reflections corresponding to the ordered phase. This ordering is further confirmed by Raman spectra and TEM images, which reveal ordering of Li and Fe ions at the octahedral sites contrasting with the relatively high degree of octahedral site disorder in the as-grown crystal. To study the effect of B-site ordering on the magnetic properties and FMR linewidth, vibrating sample magnetometry and broadband FMR measurements have been performed for both the ordered and disordered phases of lithium ferrite. The value of saturation magnetization for both phases is $\sim 290 \text{ emu/cm}^3$. A single mode FMR profile is observed for both phases with little distortion. The linewidth characteristics of the ordered and disordered phases of lithium ferrite phases are compared, and it is observed that the linewidth is independent of the cation ordering. Both the phases exhibit a low linewidth ($\sim 26 \text{ Oe}$ at 30 GHz) and the effective damping parameter for the as-grown and annealed samples is determined to be 0.0021 ± 0.0001 . © 2015 AIP Publishing LLC.

[<http://dx.doi.org/10.1063/1.4922778>]

The ferrimagnetic spinel lithium ferrite ($\text{Li}_{0.5}\text{Fe}_{2.5}\text{O}_4$ or LiFe_5O_8) has been an important candidate for microwave devices such as gyrators, circulators, isolators, and phase shifters because of its low loss at high microwave frequencies coupled with excellent magnetic properties.^{1–4} The exact origin of the loss or damping in ferrites is not precisely known, but has been attributed to relaxation mechanisms such as two-magnon scattering,^{5–7} valence exchange,⁸ fast and slow relaxing impurities,⁹ and eddy current dissipation.^{10,11} A recent theoretical study presents an approach to understand the intrinsic damping in ferrites taking into consideration the magneto-elastic coupling between spin and elastic waves and suggests an anisotropic 2nd rank damping tensor for pure perfect single crystals.¹² However, measuring such an intrinsic damping parameter in ferrites is very difficult since the experimental Gilbert damping parameter can also have contributions from some of the above mentioned relaxation mechanisms. Another factor to be considered is the strong inhomogeneous linewidth broadening in ferrite thin films, which also adds to the challenge of experimental

investigation of the damping parameter. The measurements to date on LiFe_5O_8 (LFO) provide no information about the frequency dependence of the ferromagnetic resonance (FMR) linewidth.^{13,14} In order to accurately measure the Gilbert damping parameter using Landau-Lifshitz-Gilbert (LLG) phenomenology, one needs to investigate FMR linewidth over a wide frequency range, as the experimental derivation of the damping parameter using just one frequency can lead to large systematic errors.¹⁵ In this paper, we report on detailed microstructural analysis and measurement of the effective damping parameter using broadband FMR characterization of single crystal lithium ferrite.¹⁶

The single crystal lithium ferrite material used in this study was prepared by standard flux-melt growth technique.^{17,18} The flux was prepared in a cylindrical platinum crucible by melting iron oxide and lithium carbonate with a mixture of boron oxide and bismuth oxide in a furnace with a non-uniform temperature gradient.¹⁷ Dissolution and homogenization were done at 980 °C, and the flux was mixed by a ring carrier. The saturation temperature was maintained for 24 h with the probe crystals fixed on the ring carrier. After completion of the overheating ring carrier with two

^{a)}Electronic mail: agupta@mint.ua.edu

seeds, it was immersed in the flux and rotated. Further growth occurred with slow decrease of temperature of 1–3 °C/day. At 782 °C, the carrier was lifted to break contact of the grown crystal with the solution and the furnace was cooled to room temperature at a rate of 40–50 °C/h.

We investigated the properties of both the disordered and ordered phase of LFO crystal. The as-grown LFO- S_1 spherical crystal was annealed at different temperatures in the presence of oxygen and at different cooling rates to induce ordering. The optimized conditions to observe *B*-site ordering were to anneal the as-grown sample at 600 °C for 2 h in the presence of oxygen followed by a very slow cooling at the rate of 0.5 °C/min. Higher annealing temperatures and faster cooling was found to introduce more disorder in the as-grown samples.¹⁹ In this report, the as-grown LFO crystal is referred to as S_1 , and the ordered LFO crystal obtained by annealing of S_1 under optimized conditions is referred to as S_2 . The determination of the crystal phase of the as-grown LFO- S_1 and the annealed LFO- S_2 was carried out by a standard X-ray diffraction setup (Bruker D8 Discover XRD with general area detector system, GADDS) with a cobalt radiation ($\lambda = 1.7903 \text{ \AA}$) source. Polarized Raman spectra were obtained using a Horiba T64000 Raman spectrometer with microscope attachment. The spectra were acquired from (111) crystal surfaces in backscattering configuration with 515 nm (2.41 eV) excitation. The notations HH and HV, used for scattering from the (111) surface, correspond to parallel and crossed polarization of incident and scattered light, respectively. Transmission electron microscope (TEM) cross sectional samples were prepared by mechanical polishing followed by Ar ion milling at 3.0 kV to obtain electron transparent thin areas. The zone axes (Z.A.) were different for the two samples S_1 and S_2 due to the way the bulk sample was thinned down for the microscopy study. There was no control to choose a specific crystallographic direction along which mechanical thinning could be performed. Therefore, in the thinned TEM specimen we ended up with some high symmetry zone axis within the tilting range of the holder ($\alpha = \pm 30^\circ$ and $\beta = \pm 15^\circ$). Thus, we obtained zone axis close to $\langle 100 \rangle$ type for sample S_1 and $\langle 111 \rangle$ for sample S_2 . The angle between $\langle 100 \rangle$ and $\langle 111 \rangle$ is 54.7° and cannot be tilted in our TEM holder. Magnetic properties of the crystal were determined by vibrating sample magnetometry (VSM) (Quantum Design PPMS DynaCool) at temperatures of $5 \text{ K} \leq T \leq 400 \text{ K}$ and in magnetic fields of up to 5 T. The sample was air milled and polished to the shape of a sphere of 0.5 mm diameter for FMR characterization. This was done to avoid inhomogeneous FMR linewidth broadening caused by irregularities in the shape of the sample, which would translate to an inhomogeneous demagnetization tensor. Polishing the sample to obtain as close as possible to a spherical geometry also minimizes the contribution of the two magnon scattering relaxation to the FMR linewidth, which typically is the dominant relaxation mechanism in ferrites.⁶

The ordered phase of LFO possess an inverse spinel structure with a specific 1:3 ordering of Li^{1+} and Fe^{3+} at the octahedral *B*-sites.¹⁹ The X-ray diffraction pattern of the as-grown crystal is shown in Fig. 1. As mentioned earlier, the measurements were done in a Bruker D8 Discover XRD

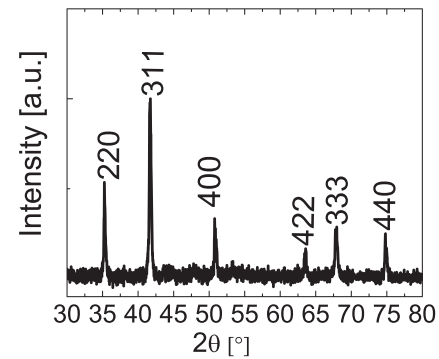


FIG. 1. Powder XRD spectra of the as-grown LFO single crystal S_1 using a Co-K α radiation source. Additional low-index weak reflections corresponding to (110), (210), and (211) are observed in the scan of the ordered phase single crystal S_2 (not shown in the plot).

with GADDS using a cobalt radiation ($\lambda = 1.7903 \text{ \AA}$) source. In order to directly compare with the reported studies and Joint Committee on Powder Diffraction Standards (JCPDS) LFO spectra,²⁰ we have recalculated the XRD peak positions corresponding to Cu-K α radiation and found there is a very good match. The lattice parameter is determined to be $8.331 \pm 0.001 \text{ \AA}$ for both LFO- S_1 and LFO- S_2 , and is very close to the bulk value of 8.337 \AA listed in JCPDS. In the as-grown LFO crystal (S_1), the LiFe_5O_8 (311) and (220) reflections are dominant along with (220), (311), (400), and (440) reflections as noted in Fig. 1. However, there are no reflections indicating the presence of any *B*-site ordering in the crystal. The X-ray diffraction study on the optimally annealed sample (S_2) indicated the presence of additional but very weak superlattice (110), (210), (211) reflections (not shown) in the XRD pattern, suggestive of ordering, along with the presence of dominant normal reflections (similar to those present in S_1). The intensities of the low-index superlattice peaks are very small as compared to the strong (311) or (220) peaks, and qualitatively matches with what is expected based on the JCPDS LFO spectra.

The cation ordering after annealing has been conclusively confirmed by Raman Spectroscopy data, as shown in Fig. 2. The polarized Raman spectra also confirms the conversion of the crystal S_1 from the disordered beta phase to the ordered

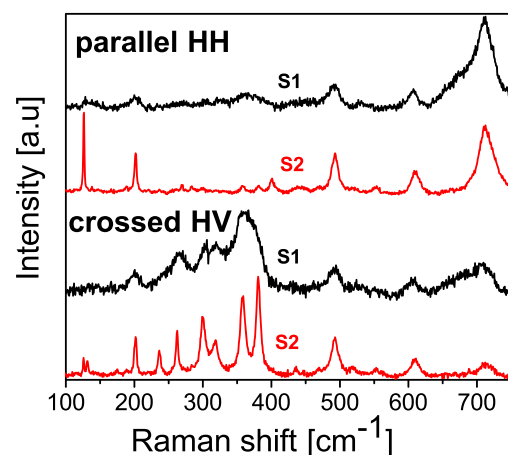


FIG. 2. Polarized Raman spectra for S_1 (disordered) and S_2 (ordered) phases of the LFO single crystal.

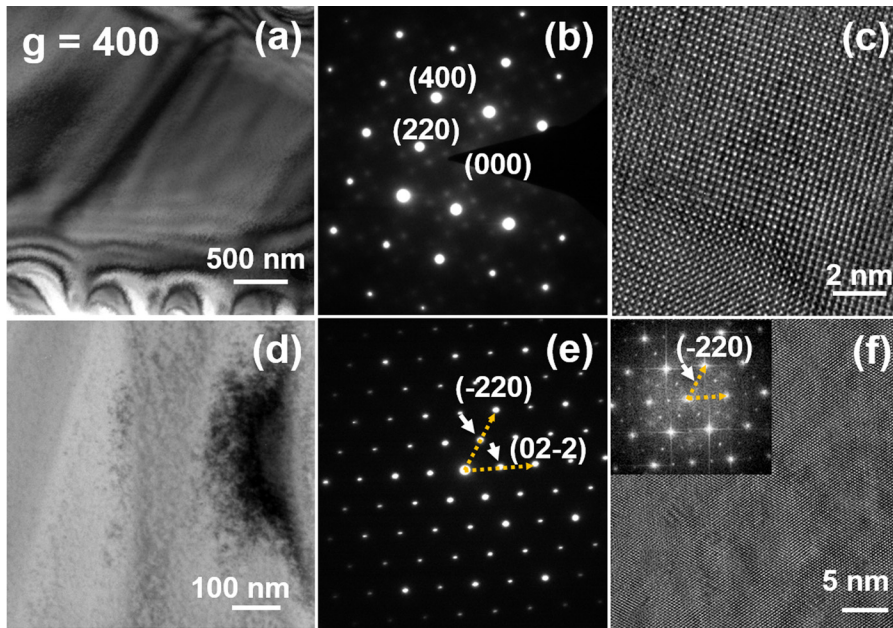


FIG. 3. (a)–(c) and (d)–(f) TEM BF images, diffraction pattern, and HRTEM images for sample S_1 and S_2 , respectively. While the as-grown sample S_1 shows only short range ordering, the annealed sample S_2 shows strong ordering due to Li^+ and Fe^{3+} in 1:3 ratio at the octahedral 16d positions.

alpha phase in S_2 , consistent with previously reported Raman study on LFO crystals.²¹ In the ordered ($P4_332$) phase, $6A_1 + 14E + 20F_2$ phonon modes are allowed in the Raman spectra, whereas for the disordered ($Fd-3m$) phase, the number of Raman allowed phonons is only five ($A_{1g} + E + 3F_{2g}$). In addition, one expects strong broadening of the Raman bands of the disordered phase. Therefore, the ordered and disordered phases of LFO can easily be distinguished by their Raman spectra. We have also studied the as-grown and annealed crystals using TEM. Fig. 3(a) shows TEM bright field (BF) image of the as-grown crystal (S_1) with $g = \langle 400 \rangle$ diffracting vector. No strain contrast associated with either line or planar defects are observed. The diffraction pattern (Fig. 3(b)) shows single crystalline pattern with weak and diffused superlattice (SL) spots. Only $\langle 100 \rangle$ and $\langle 110 \rangle$ and its odd multiples SL spots are present. The $\frac{1}{2}\langle 400 \rangle$ SL spots are absent. This suggests that the periodicity of octahedral planes ordering is along the $\langle 100 \rangle$ direction and only in the short range. Fig. 3(c) is the HRTEM image of the sample. The TEM images and electron diffraction patterns of the annealed sample are shown in Figs. 3(d)–3(f). Fig. 3(d) is the bright field image with $g = \langle 004 \rangle$ type diffracting vector. Similar to the as grown sample, the presence of dislocations or other types of crystallographic defects are not observed. The diffraction pattern along $\langle 111 \rangle$ direction is shown in Fig. 3(e), showing strong SL spots marked with the arrow in-between the main spots. Fig. 3(f) is the HRTEM image along $\langle 111 \rangle$ Z.A. and the Fourier transform image in the inset of Fig. 3(f) also show the presence of SL spots. Both the HRTEM images indicate absence of any stacking faults and antiphase boundaries within the areas investigated under TEM. Based on the TEM results, we can conclude that the LFO single crystal is of high quality. Partial B -site cation ordering is present in the as-grown crystal (S_1) and complete ordering is obtained after anneal (S_2) due to Li^+ and Fe^{3+} in 1:3 ratio at the octahedral 16d positions.

Fig. 4 shows the magnetic hysteresis loops of the annealed crystal (sample S_2) versus applied DC magnetic field at two different temperatures. The saturation

magnetization values obtained from the MH-loops are 290 emu/cm^3 and 320 emu/cm^3 at 300 K and 5 K, respectively. The bulk magnetization value for lithium ferrite is $2.5 \mu_B/\text{formula unit}$, corresponding to $\sim 320 \text{ emu/cm}^3$. The saturation magnetization value of the as-grown crystal at room temperature (not shown) is similar to that of the crystal after annealing (290 emu/cm^3). This is expected since the distribution of Fe^{3+} does not change between the tetrahedral and octahedral sites.²²

Broadband FMR was used to study the dynamic magnetic properties of the LFO single crystal. The spherical single crystal was placed in a plastic holder and was positioned on top of a coplanar waveguide (CPW) and the transmitted signal was detected by a microwave diode while at a fixed frequency the quasi static field was swept at room temperature. A pair of coils was used to modulate a small AC magnetic field on top of the quasi static field, which caused the signal to oscillate and enabled the detection of signal by means of the lock-in technique. The derivative of the transmitted power with respect to the DC field was measured as

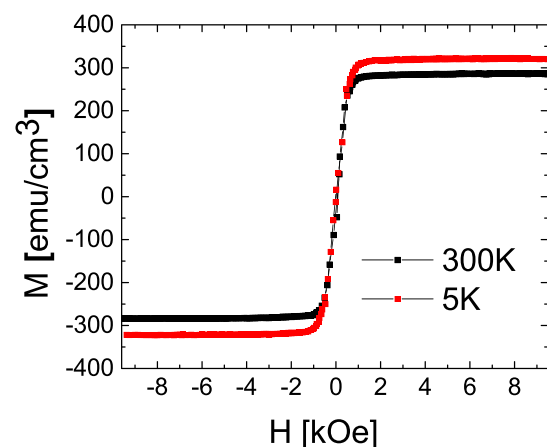


FIG. 4. The magnetization as a function of applied magnetic field (M-H) plot for the S_2 sample at 5 K and 300 K.

the FMR spectra.¹⁶ The FMR spectra was fitted using the derivative of a Lorentzian function, which included absorption and dispersion contributions to extract the resonance field (H_{res}) and the FMR linewidth (ΔH).²³ Fig. 5 shows the measured FMR resonance field as a function of frequency ranging from 9–40 GHz in steps of 1 GHz for the ordered phase of the LFO crystal. An example of FMR spectrum, obtained at 30 GHz, is shown as an inset in Fig. 5, with a linewidth of 26 Oe. As evident, the FMR profile is quite clean, with little distortion or additional structure. No attempt was made to orient the crystal with respect to the external field; thus, the observed linewidth is likely larger than the smallest obtainable linewidth.²⁴

For a spherical ferrite crystal with vanishing magnetic anisotropy, the uniform FMR mode of resonance field H_{res} is given by²⁵

$$f = \gamma' H_{res}, \quad (1)$$

where f is the resonance frequency and γ' is the gyromagnetic ratio. The value obtained from the fitted data (shown in Fig. 5) for γ' is 2.768 ± 0.003 GHz/kOe for the S_1 sample and 2.784 ± 0.006 GHz/kOe for the ordered S_2 sample. The reported error margins only take statistical errors into account. It is noteworthy to mention that there usually exist large systematic error margins in measuring γ' ,²⁶ which are minimized using broadband FMR measurements.

No previous report on the value of the gyromagnetic ratio for lithium ferrite was found in the literature. The previous studies of FMR properties of lithium ferrite single crystals or thin films were all done at one or two nominal frequencies,^{2,6,13,14,24,25,27,28} which lead to large uncertainties in the experimentally determined gyromagnetic ratio and damping parameter values. However, broadband determined gyromagnetic ratios of barium ferrite single crystal,²⁹ $Ba_2Zn_2Zr_xFe_{12-x}O_{22}$ single crystal³⁰ are 2.8 GHz/kOe and for yttrium iron garnet (YIG) films³¹ 2.84 GHz/kOe, i.e.,

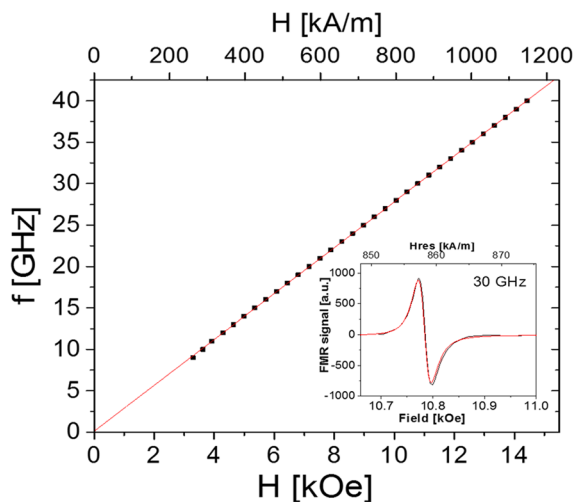


FIG. 5. Frequency dependence of FMR resonance field fitted with $\omega = \gamma H_{res}$ for samples S_1 and S_2 , the resonance fields of both samples are essentially identical; therefore one cannot distinguish them in the figure. The inset shows the raw FMR signal for LFO- S_2 obtained at 30 GHz showing a linewidth of 26 Oe, the fit of the data is shown in red.

close to the value we have found for lithium ferrite. The close to linear frequency dependence of linewidth for both S_1 and S_2 samples, is fitted as shown in Fig. 6 using the equation³²

$$\Delta H(f) = \Delta H_0 + \frac{2}{\sqrt{3}} \frac{\alpha}{\gamma'} f, \quad (2)$$

where α is the Gilbert damping parameter and ΔH_0 is the linewidth offset at zero frequency caused by microstructural inhomogeneities. The fitted value of the damping is 0.0021 ± 0.0001 for both the as-grown and annealed samples. It is clear that the frequency dependence of the linewidth values and thus the damping parameter do not change significantly with the B -site cation ordering in the LFO single crystal.

There are no reports on the value of damping parameter for lithium ferrite in the literature. However, one can compare linewidth values at one or two specific frequencies with previous reports. For example, Spencer *et al.* have found the linewidth to be 1.45 Oe at 10.4 GHz (Ref. 13) for ordered lithium ferrite single crystal and Denton and Spencer have reported linewidths in the range of 1–4 Oe for partially ordered lithium ferrite single crystal at 10.88 GHz depending on the direction of quasi-static field with respect to the crystallographic orientations.²⁴ While the experimentally measured linewidth values presented in this paper are 7 Oe and 3.5 Oe at 10 GHz for S_1 and S_2 samples, respectively, which are not far from the previous results. One can also compare the damping parameter of lithium ferrite single crystals, with those reported for YIG single crystals, which are typically of the order 0.0002,³¹ i.e., one order of magnitude smaller than the value reported in this work.

In summary, we have characterized flux-grown spinel $LiFe_5O_8$ single crystals by XRD, polarized Raman spectroscopy, TEM, and VSM to closely examine the structural and magnetic properties for both the disordered and ordered phases. After careful air milling and polishing to produce a spherical sample, we have been able to obtain a single mode FMR profile, which is clean with little distortion. The

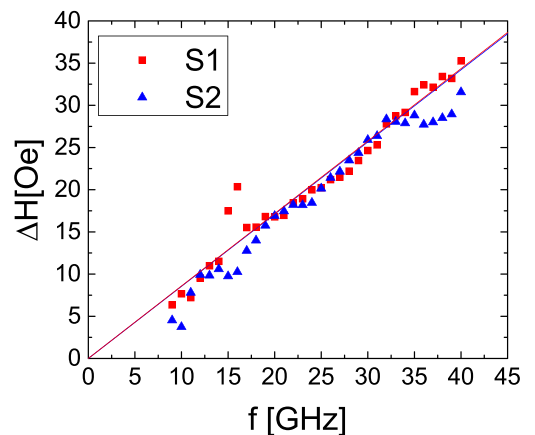


FIG. 6. FMR linewidth dependence on frequency for samples S_1 and S_2 . The data are fitted using Eq. (2) giving a value of 0.002 for the damping parameter of both samples.

damping parameter of LiFe_5O_8 has been determined using the broadband frequency dependence of the FMR linewidth.

This work has been supported by NSF Grant No. ECCS-1102263. Tim Mewes and Behrouz Khodadadi would like to acknowledge support by the NSF-CAREER Award No. 0952929. R. Datta and B. Loukya sincerely acknowledge ICMS for providing advanced microscopy facility and funding. We thank Sahar Keshavarz, Archana Panikar, Stefan Kingler, and Jamileh Beik Mohammadi for help with the experimental work.

- ¹W. V. Aulock, *Handbook of Microwaves Ferrites* (Materials Academic Press, New York, NY, USA, 1965).
- ²G. O. White and C. E. Patton, *J. Magn. Magn. Mater.* **9**, 299 (1978).
- ³C. E. Patton, C. A. Edmondson, and Y. H. Liu, *J. Appl. Phys.* **53**, 2431 (1982).
- ⁴A. Goldman, *Modern Ferrite Technology*, 2nd ed. (Springer, US, Pittsburg, 2006).
- ⁵N. Li, S. Schaefer, R. Datta, T. Mewes, T. M. Klein, and A. Gupta, *Appl. Phys. Lett.* **101**, 132409 (2012).
- ⁶N. Mo, Y. Y. Song, and C. E. Patton, *J. Appl. Phys.* **97**, 093901 (2005).
- ⁷S. S. Kalarickal, N. Mo, P. Krivosik, and C. E. Patton, *Phys. Rev. B* **79**, 094427 (2009).
- ⁸A. G. Flores, V. Raposo, L. Torres, and J. Iniguez, *J. Appl. Phys.* **85**, 2293 (1999).
- ⁹A. J. Heeger, T. G. Blocker, and S. K. Ghosh, *Phys. Rev.* **134**, A399 (1964).
- ¹⁰S. Yamada and E. Otsuki, *J. Appl. Phys.* **81**, 4791 (1997).
- ¹¹J. R. Truedson, K. D. McKinstry, P. Kabos, and C. E. Patton, *J. Appl. Phys.* **74**, 2705 (1993).
- ¹²C. Vittoria, S. D. Yoon, and A. Widom, *Phys. Rev. B* **81**, 014412 (2010).
- ¹³E. G. Spencer, D. A. Lepore, and J. W. Nielsen, *J. Appl. Phys.* **39**, 732 (1968).

- ¹⁴G. A. Petrovskii and V. N. Berzhanskii, *Sov. Phys. Solid State* **13**, 495 (1971).
- ¹⁵C. K. A. Mewes and T. Mewes, "Relaxation in magnetic materials for spintronics," in *Handbook of Nanomagnetism-Applications and Tools* (Pan Stanford Publishing, 2015).
- ¹⁶S. Keshavarz, Y. L. Xu, S. Hrdy, C. Lemley, T. Mewes, and Y. P. Bao, *IEEE Trans. Magn.* **46**, 1541 (2010).
- ¹⁷L. N. Bezmaternykh, V. G. Mashchenko, N. A. Sokolova, and V. L. Temerov, *J. Cryst. Growth* **69**, 407 (1984); L. N. Bezmaternykh and N. Sokolova, patent of the Russian Federation 2072004 (20 January 1997).
- ¹⁸J. P. Remeika and R. L. Comstock, *J. Appl. Phys.* **35**, 3320 (1964).
- ¹⁹P. B. Braun, *Nature* **170**, 1123 (1952).
- ²⁰JCPDS Card No. 17-115.
- ²¹M. N. Iliev, V. G. Ivanov, N. D. Todorov, V. Marinova, M. V. Abrashev, R. Petrova, Y. Q. Wang, and A. P. Litvinchuk, *Phys. Rev. B* **83**, 174111 (2011).
- ²²G. T. Rado and V. J. Folen, *J. Appl. Phys.* **31**, 62 (1960).
- ²³C. J. Oates, F. Y. Ogrin, S. L. Lee, P. C. Riedi, G. M. Smith, and T. Thomson, *J. Appl. Phys.* **91**, 1417 (2002).
- ²⁴R. T. Denton and E. G. Spencer, *J. Appl. Phys.* **33**, 1300 (1962).
- ²⁵U. Ozgur, Y. Alivov, and H. Morkoc, *J. Mater. Sci.: Mater. Electron.* **20**, 789 (2009).
- ²⁶J. M. Shaw, H. T. Nembach, T. J. Silva, and C. T. Boone, *J. Appl. Phys.* **114**, 243906 (2013).
- ²⁷G. M. Argentina and P. D. Baba, *IEEE Trans. Microwave Theory Tech.* **MT22**, 652 (1974).
- ²⁸W. G. Nilsen, R. L. Comstock, and J. P. Remeika, *J. Appl. Phys.* **37**, 1224 (1966).
- ²⁹S. V. Lebedev, C. E. Patton, M. A. Wittenauer, L. V. Saraf, and R. Ramesh, *J. Appl. Phys.* **91**, 4426 (2002).
- ³⁰J. Jalli, Y.-K. Hong, S. Bae, J.-J. Lee, G. S. Abo, J.-H. Park, B.-C. Choi, T. Mewes, S.-G. Kim, S.-H. Gee, I.-T. Nam, and T. Tanaka, *J. Appl. Phys.* **109**, 07A509 (2011).
- ³¹C. Hahn, G. de Loubens, O. Klein, M. Viret, V. V. Naletov, and J. B. Youssef, *Phys. Rev. B* **87**, 174417 (2013).
- ³²B. Heinrich, in *Ultrathin Magnetic Structures III*, edited by J. A. Bland and B. Heinrich (Springer, Berlin Heidelberg, 2005), p. 143.